Characterization of New Infrared Nonlinear Optical Material with High Laser Damage Threshold, $Li_2Ga_2GeS_6$

Youngsik Kim,[†,‡] In-seok Seo,[†] Steve W. Martin,*[,†] Jaewook Baek,[§] P. Shiv Halasyamani,[§] Nachiappan Arumugam,[⊥] and Hugo Steinfink[⊥]

Department of Materials Science and Engineering, Iowa State University, Ames, Iowa 50011-2300, Department of Chemistry, University of Houston, Houston, Texas 77204-5003, Texas Materials Institute, Department of Chemical Engineering, and The University of Texas at Austin, Austin, Texas 78712

Received March 12, 2008. Revised Manuscript Received July 8, 2008

A new thio-germanium sulfide $Li_2Ga_2GeS_6$ has been synthesized for the first time and its structure was found to be isomorphous with $AgGaGeS_4$, which is well-known as a promising infrared NLO material. The host structure is built of GaS_4 tetrahedra linked by corners to GeS_4 tetrahedra to create a 3D framework forming tunnels along the *c*-axis, in which the Li^+ ions are located. The second harmonic generation (SHG) efficiency determined on powders of $Li_2Ga_2GaS_6$ is ~200 times larger than that of α-SiO_2. Unlike $AgGaS_2$ and $AgGaGeS_4$, $Li_2Ga_2GeS_6$ was observed to be very stable under prolonged Nd:YAG 1.064 μm laser pumping, indicative of a large improvement in laser damage threshold. This new material could supplant Ag phases in the next generation of high-power infrared NLO applications.

Introduction

One of the simplest ways to design new types of lasers is to convert the frequency of known lasers into new frequencies through nonlinear optical (NLO) materials. The development of numerous NLO crystals such as β-BaB_2O_4 (BBO),[1,2] LiB_3O_5 (LBO),[3] $AgGaS_2$ (AGS),[4−7] and $AgGaGeS_4$ (AGGS)[8−12] has led to significant advances in the laser device applications from ultraviolet to infrared spectral wavelengths. Although oxide-based NLO materials have generally been applied in ultraviolet (UV) and visible high power applications because of their high laser damage thresholds and their good transmission from the near-infrared (NIR) to UV range (0.16−5.5 μm), sulfur-based NLO materials have been largely used for frequency conversion in the infrared (IR) spectral range because of their improved IR transmission region (0.4−15 μm). More recently, a new approach to design all-solid state mid-IR laser sources from the widely used solid-state Nd:YAG laser and a set of frequency converters have been reported.[13] The critical part of this system is the frequency converters (NLO crystals) which should efficiently shift the 1.064 μm light of the Nd:YAG laser to wavelengths beyond 4 μm. Unfortunately, most of the reported infrared NLO crystals have some serious limitations. The major drawbacks of IR frequency converters with the Nd:YAG laser radiation pumping are the high value of the optical losses at short wavelengths due to their poor transparency[6] and low laser damage thresholds because of the low energy band gaps.[14] For example, $AgGaS_2$ is the most common and technologically mature material for NLO applications in the mid-IR range based on such characteristics as the second harmonic generation (SHG) coefficient, transparency range, single-crystal growth, and absorption coefficient. However, its application in the mid-infrared region is limited because of its low laser damage threshold.[15] The search for better infrared NLO materials has resulted in the development of the quaternary compound $AgGaGeS_4$,[8] which is formed by the solid solution between the parent $AgGaS_2$ and GeS_2 in which the laser damage threshold increased with the addition of GeS_2 to $AgGaS_2$. The improved laser damage threshold in $AgGaGeS_4$ has made it a promising alternative to the widely used $AgGaS_2$ for a frequency down-converter with a Nd:YAG laser application pumping as well as many other applications.[8,10,15]

* Author to whom correspondence should be addressed. E-mail: swmartin@iastate.edu.
† Iowa State University.
‡ Current address: Texas Materials Institute, The University of Texas at Austin, Austin, Texas 78712.
§ University of Houston.
⊥ The University of Texas at Austin.

(1) Chen, C.; Wu, B.; Jiang, A.; You, G. *Sci. Sin.* **1985**, *B28*, 235.
(2) Bromley, L. J.; Guy, A.; Hanna, D. C. *Opt. Commun.* **1988**, *67*, 316.
(3) Chen, C.; Wu, Y. J. *Opt. Soc. Am.* **1989**, *B6*, 616.
(4) Chemla, D. S.; Kupecek, P. J.; Robertson, D. S.; Smith, R. C. *Opt. Commun.* **1971**, *3*, 29.
(5) Boyd, G. D.; Kasper, H.; McFee, J. M. *IEEE J. Quantum Electron.* **1971**, *QE-7*, 563.
(6) Bhar, G. C.; Smith, R. C. *Phys. Status Solidi, A* **1972**, *13*, 157.
(7) Ruderman, W.; Maffetone, J.; Zelman, D.; Poirier, D. *Mater. Res. Soc. Symp. Proc.* **1998**, *484*, 519.
(8) Badikov, V. V.; Tyulyupa, A. G.; Shevyrdyaeva, G. S.; Sheina, S. G. *Inorg. Mater.* **1991**, *27*, 177. [Translation from *Dokl. Akad. Nauk SSSR, Neorg. Mater.* **1991**, *27*, 248.
(9) Andreev, Yu.M.; Badikovz, V. V.; Voevodin, V. G.; Geiko; L. G.; Geiko, P. P.; Ivashchenko, M. V.; Karapuzikov, A. I.; Sherstov, I. V. *Quantum Electron.* **2001**, *31*, 1075.
(10) Petrov, V.; Badikov, V.; Shevyrdyaeva, G.; Panyutin, V.; Chizhikov, V. *Opt. Mater.* **2004**, *26*, 217.
(11) Das, S.; Ghosh, C.; Gangopadhyay, S.; Andreev, Y. M.; Badikov, V. V. *Jpn. J. Appl. Phys.* **2006**, *45*, 5795.
(12) Pobedimskaya, E. A.; Alimova, L. L.; Belov, N. V.; Badikov, V. V. *Sov. Phys. Dokl.* **1981**, *26*, 259. [Translation from *Dokl. Akad. Nauk SSSR* **1981**, *257*, 611]. Note: Table 2 in this reference lists the coordinates of a phase labeled $AgGaGeS_4$. However, the number of atoms in the Wyckoff positions of *Fdd*2 listed in that table lead to the stoichiometry $Ag_{1.28}(Ge_{0.5}Ga_{0.5})_2(Ge_{0.5}Ga_{0.5})S_6$, comparable to the stoichiometry reported here, $Li_2Ga_2GeS_6$.
(13) Hopkins, F. K.; Fernelius, N. C.; Goldstein, J. T.; Zelmon, D. E.; Leininger, C. A. *Proc. SPIE* **2005**, *5912*, 591202–1.
(14) Atuchin, V. V.; Kidyarov, B. I.; Pervukhina, N. V. *Comput. Mater. Sci.* **2006**, *37*, 507.
(15) Schunemann, P. G. *Proc. SPIE* **2006**, *6103*, 610303.

10.1021/cm8007304 CCC: $40.75
Published on Web 08/21/2008

In our previous research efforts,[16] thioborate materials based on boron sulfide had been proposed for a new class of infrared NLO materials. It was found that thioborate crystals based on $(BS_3)^{3-}$ structural units showed strong SHG effects when pumped with the Nd:YAG laser, a wide transparency range from the visible to the mid-IR region (0.35−10 μm), and especially strong laser damage threshold compared to other sulfur-based NLO materials. However, the number of the reported thioborate crystals with noncentrosymmetric structures is extremely limited.[16] In addition, the experimental difficulty of synthesizing new thioborate crystals[16,17] have retarded further progress in developing thioborate crystals as new infrared NLO materials.

The extensive search for new and better infrared NLO materials, especially sulfur-based materials, has continued and these efforts have yielded a new sulfide compound, $Li_2Ga_2GeS_6$. Its structure was found to be noncentrosymmetric which is a necessary criterion for NLO properties. In addition, the structure of $Li_2Ga_2GeS_6$ was later shown to be isostructural with $AgGaGeS_4$, (v. i.) which, as discussed above, has been found to be a promising NLO material for IR applications. In this paper we report the crystal structure and preliminary optical characterization of a new thiogermanium-galium phase, $Li_2Ga_2GeS_6$. This material is phase-matchable with a large SHG efficiency of ∼200 × α-SiO_2 when probed at Nd:YAG 1.064 μm laser pumping. In addition, there is a large improvement in the laser damage threshold of $Li_2Ga_2GeS_6$ compared with that of $AgGaGeS_4$.

Experimental Section

Preparation. Single crystals of what was eventually identified as $Li_2Ga_2GeS_6$ were obtained from 1 g batches of the reactants, Li_2S (Alfa, 99.9%) GeS_2 (prepared from the elements),[18] and Ga_2S_3 (Alfa, 99.9%) mixed in the ratio of 1:4:1. The mixture was placed inside a predried carbon-coated quartz tube inside an oxygen- and water-free glovebox (<1 ppm O_2 and <1 ppm H_2O), and then sealed under vacuum. The sealed tube and contents were heated according to the temperature profile

$$\mathrm{RT} \xrightarrow{10\ \mathrm{h}} 950\ °\mathrm{C}\ (5\ \mathrm{h}) \xrightarrow{7\ \mathrm{h}} 750\ °\mathrm{C} \xrightarrow{100\ \mathrm{h}} 500\ °\mathrm{C}\ (20\ \mathrm{h}) \xrightarrow{\text{air-quench}} \mathrm{RT} \quad (1)$$

A mass of the crystalline phase (major phase) was observed on the bottom of the quartz tube. This crystalline phase was completely separated and single crystals were selected for X-ray diffraction data collection. A yellowish-white powder was obtained from grinding the remaining phase. Powder X-ray diffraction data were collected on a Scintag XDS2000 diffractometer using Cu Kα (λ = 1.5406 Å); it was operated at 40 kV and 30 mA with step size 0.02 (See Supporting Information).

Single-Crystal X-ray Diffraction Measurements. The crystal evaluation and data collection were performed at 193 K on a Bruker CCD-1000 diffractometer with Mo Kα (λ = 0.71073 Å) radiation and detector to crystal distance of 5.03 cm. The crystal was twinned, so no initial cell constants were obtained from three series of ω scans at different starting angles. While the profiles of reflections were sharp, at least 4 crystallites were found using the program RLATT routine in the SHELXTL program.[19] The data were collected using the full sphere algorithm. Four sets of frames with 0.3° scan in ω with an exposure time 20 s per frame were used. The reflections belonging to one individual crystallite were separated from all the data sets using RLATT and integrated with SAINT routines.[19] The systematic absences in the diffraction data were consistent with the unique space group *Fdd*2 (No. 43). The positions of all atoms were found by the direct method. All atoms were refined in a full-matrix least-squares procedure using absorption corrected intensities using SADABS[20] and anisotropic displacement parameters. Details of the data collection and structure refinement are listed in Table 1. The final atomic positions and the equivalent displacement parameters are in Table 2.

IR Spectroscopy. The mid- and far-infrared absorption spectra of the polycrystalline powder were recorded in the range of 4000 to 400 cm^{-1} and 750 to 150 cm^{-1}, respectively, with the use of a

Table 1. Crystal Data and Details of the Structure Refinement for $Li_2Ga_2GeS_6$

empirical formula	$Li_2Ga_2GeS_6$
fw	411.33
T (K)	293(2)
radiation	Mo$K\alpha$ (λ = 0.71073 Å)
cryst syst	orthorhombic
space group	*Fdd*2 (No. 43)
a (Å)	11.943(5)
b (Å)	22.590(8)
c (Å)	6.805(2)
α (deg)	90
β (deg)	90
γ (deg)	90
V (Å^3)	1835.9(12)
Z	8
d_{calcd} (Mg/m^3)	2.976
abs coeff (mm^{-1})	10.360
F(000)	1544
cryst size (mm^3)	0.20 × 0.15 × 0.15
θ range for data collection (deg)	3.56−28.25
index ranges	$0 \le h \le 15$, $0 \le k \le 29$, $-8 \le l \le 8$
no. of reflns collected	4190
no. of independent reflns	951 [R(int.) = 0.053]
completeness to θ = 28.25° (%)	98.7
abs corrn	SADABS
min/max transmission	0.055991
refinement method	full-matrix least-squares on F^2
data/restraints/params	951/1/46
GOF on F^2	1.05
final R indices [$I > 2\sigma(I)$][a]	R_1 = 0.0459, wR_2 = 0.1130
R indices (all data)[a]	R_1 = 0.0459, wR_2 = 0.1130
absolute structure parameter	0.09(3)
largest diff. peak and hole (e Å^{-3})	1.278 and −1.106

[a] $R_1 = \sum||F_o| - |F_c||/\sum|F_o|$ and $wR_2 = \{\sum[w(F_o^2 - F_c^2)^2]/\sum[w(F_o^2)^2]\}^{1/2}$.

Table 2. Atomic Coordinates (× 10^4) and equivalent Isotropic Displacement Parameters (Å^2 × 10^3) for $Li_2Ga_2GeS_6$

	x	y	z	U_{eq}[a]
Ga(1)/M(1)	1273(1)	3627(1)	9408(2)	10(1)
Ge(1)/M(2)	0	1/2	9149(2)	13(1)
S(1)	493(2)	4237(1)	7218(4)	16(1)
S(2)	577(2)	3698(1)	12436(4)	16(1)
S(3)	946(2)	2706(1)	8413(4)	17(1)
Li(1)	1700(40)	4530(20)	4020(70)	97(12)

[a] U_{eq} is defined as one third of the trace of the orthogonalized U_{ij} tensor.

(16) Kim, Y.; Martin, S. W.; Ok, K. M.; Halasyamani, P. S. *Chem. Mater.* **2005**, *17*, 2046.
(17) Krebs, B. *Phosphorus, Sulfur, Silicon Relat. Elem.* **2001**, *168*, 11.
(18) Kim, Y.; Saienga, J.; Martin, S.W. *J. Phys. Chem. B* **2006**, *110*, 16318.
(19) All software and sources of the scattering factors are contained in the program library: Sheldrick, G. *SHELXTL*, version 5.1; Bruker Analytical X-ray Systems: Madison, WI.
(20) Sheldrick, G. M. *SHELXTL*, version 6.14; Bruker Analytical X-ray Instruments: Madison, WI, 2003.

Bruker IFS 66 v/s spectrometer. Two milligrams of each sample were ground with 100 mg of CsI into a fine powder and pressed into pellets for transmission measurement. The IR spectra typically were obtained using 32 scans at a 4 cm^{-1} resolution.

UV/VIS/NIR Spectroscopy. The UV/VIS/NIR spectra were recorded in the range of 200 to 3000 nm at room temperature using a PE Lambda-19 spectrometer. The UV/VIS/NIR spectra of the samples were obtained using the KBr pellet method. Two milligrams of the sample were ground with 100 mg of KBr, previously dried at 300 °C, and pressed into pellets for spectroscopic measurements.

Second-Harmonic Generation Measurements. The second-order nonlinearity of the powder sample of $Li_2Ga_2GeS_6$ was examined using a modified Kurtz-NLO system with a 1.064 μm Nd:YAG laser.[27] Polycrystalline $Li_2Ga_2GeS_6$ was ground and sieved into distinct particle size ranges, <20, 20−45, 45−63, 63−75, 75−90, and 90−125 μm. They were placed in separate capillary tubes. To make relevant comparisons with known SHG materials, α-SiO_2 and $LiNbO_3$ were ground and sieved into the same particle size ranges and placed into separate capillary tubes. For $AgGaS_2$ and $AgGaGeS_4$ samples, the particle sizes ranging from 45 to 63 μm were used for the SHG efficiency measurements. The samples were exposed to a Nd:YAG laser at 1.064 μm and the filtered SHG light, 0.532 μm, was collected in reflection and detected by a photomultiplier tube (Oriel Instruments). A digital oscilloscope (Tektronix TDS 3032) was used to display the SHG signal. The powder SHG properties of the samples were expressed as the comparative intensity $[I^{2\omega}/I^{2\omega}_{SiO_2}]$ of α-SiO_2.

Results and Discussion

The crystal structure of $Li_2Ga_2GeS_6$ was determined by single crystal X-ray diffraction methods. It crystallizes in the non-centrosymmetric orthorhombic space group *Fdd*2 (No. 43), $a = 11.943(5)$ Å, $b = 22.590(8)$ Å, $c = 6.805(2)$ Å, and $Z = 8$. Its crystal structure was found to be an isomer of $AgGaGeS_4$[12]* which is a well-known infrared NLO material, but $AgGaGeS_4$ has slightly different unit cell dimensions due to the slightly larger Ag^+ ion. There are two tetrahedral sites, M1 and M2, for Ga and Ge atoms in the structure of $Li_2Ga_2GeS_6$. However, the question of ordering of Ga and Ge on the tetrahedral sites is not possible to be answered by this X-ray investigation because the scattering factors of Ga and Ge are so similar with respect to X-rays. Initially M1, position 16b of the space group and M2, position 8a, were labeled arbitrarily. At the conclusion of the refinement the valence bond sums (VBS) around the atoms indicated that M1 is Ga, VBS = 3.38 and M2 is Ge, VBS = 3.64.[21] In other similar sulfide compounds, such as $AgGaGeS_4$[12] and $KGaGeS_4$,[22] Ga and Ge were reported to randomly occupy both tetrahedral sites due to their similar sizes and coordination preferences. The results of our crystal structure determination indicate that the site occupancies in major part are by a single atomic species as shown by the valence bond calculations.

Figure 1 shows the unit-cell crystal structure of $Li_2Ga_2GeS_6$ parallel to the *c*-axis. In this view of this structure GeS_4 tetrahedra are isolated and are connected by four GaS_4 tetrahedra (Figure 1) to form the 3D framework. The GeS_4 tetrahedra are formed by two S3 and two S1 atoms. Each S3 corner atom of each GeS_4 tetrahedron is shared by one GaS_4 and two LiS_4 tetrahedra, whereas each S1 is part of one GeS_4 tetrahedron and one LiS_4 tetrahedron. The GaS_4 tetrahedra form an infinite chain by corner sharing of two S2 atoms; two different chains exist in the *a*−*c* plane forming an acute angle with each other and are cross connected by GeS_4 tetrahedra, Figure 2a. The Li atoms in distorted tetrahedral coordination form an infinite chain parallel to the *c*-axis and perpendicular to the *a*−*b* plane by corner sharing of the S3 atoms, Figure 2b.

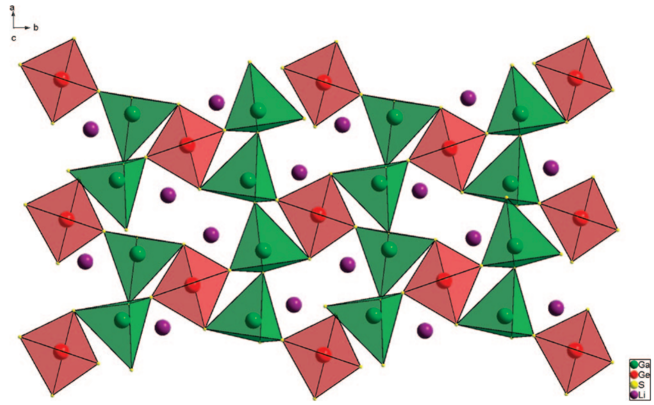

Figure 1. View of the $Li_2Ga_2GeS_6$ structure parallel to [001].

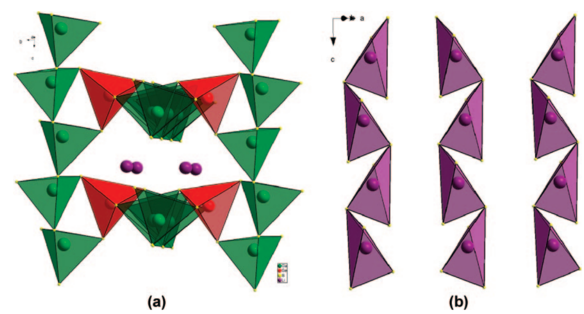

Figure 2. (a) View of the structure of $Li_2Ga_2GeS_6$ projected onto the (101) emphasizing GaS_4 chains. (b) View of the structure on to the (110) plane emphasizing the lithium tetrahedral chains.

The interatomic distances and angles for $Li_2Ga_2GeS_6$ are listed in Table 3. The bond lengths of the main group elements with sulfur are similar to those observed in $AgGaGeS_4$.[12] The lithium atom occupies the 16b position of *Fdd*2 but shows a relatively large displacement parameter indicative of possible lithium disorder. Least squares refinement on its occupancy converges to 0.53(9) with a reasonable displacement parameter. The charge imbalance due to the Li vacancies is most likely compensated by a sulfur vacancy. However the refinement to look for such a small electron density difference was not successful. The R_1 values of the two models remains the same and we choose to report the charge-balanced stoichiometry.

Figure 3 shows the IR spectrum of $Li_2Ga_2GeS_6$ compared to that of the $AgGaGeS_4$ and $AgGaS_2$. The lattice vibrations of $AgGaS_2$ were investigated by IR and Raman spectra[23]

(21) Wills, A. S.; Brown, I. D. *VALIST 1.0*; Commissariat à l'Énergie Atomique: Saclay, France, 1999.
(22) Wu, P.; Lu, Y.; Ibers, J.A. J. *Solid State Chem.* **1992**, *97*, 383.
(23) Van der Ziel, J. P.; Meixner, A. E.; Kasper, H. M.; Ditzenberger, J. A. *Phys. Rev. B* **1974**, *9*, 4286.

Table 3. Selected Bond Lengths (Å) and Angles (deg) for $Li_2Ga_2GeS_6$[a]

Ga(1)−S(2)$^{\#1}$	2.219(3)	S(2)$^{\#1}$−Ga(1)−S(3)	112.71(10)
Ga(1)−S(3)	2.223(3)	S(2)$^{\#1}$−Ga(1)−S(2)	101.51(11)
Ga(1)−S(2)	2.228(3)	S(3)−Ga(1)−S(2)	106.47(10)
Ga(1)−S(1)	2.233(3)	S(2)$^{\#1}$−Ga(1)−S(1)	113.81(10)
		S(3)−Ga(1)−S(1)	107.51(10)
Ge(1)−S(1)	2.246(3)	S(2)−Ga(1)−S(1)	114.65(10)
Ge(1)−S(1)$^{\#2}$	2.246(3)		
Ge(1)−S(3)$^{\#3}$	2.258(3)	S(1)−Ge(1)−S(1)$^{\#2}$	108.42(14)
Ge(1)−S(3)$^{\#4}$	2.258(3)	S(1)−Ge(1)−S(3)$^{\#3}$	104.70(9)
		S(1)$^{\#2}$−Ge(1)−S(3)$^{\#3}$	111.59(9)
Li(1)−S(3)$^{\#1}$	2.53(5)	S(1)−Ge(1)−S(3)$^{\#4}$	111.59(9)
Li(1)−S(2)$^{\#7}$	2.54(5)	S(1)$^{\#2}$−Ge(1)−S(3)$^{\#4}$	104.70(9)
Li(1)−S(3)$^{\#8}$	2.61(5)	S(3)$^{\#3}$−Ge(1)−S(3)$^{\#4}$	115.77(16)
Li(1)−S(1)	2.69(5)		

[a] Symmetry transformations used to generate equivalent atoms: #1 $x + 1/4, -y + 3/4, z - 1/4$; #2 $-x, -y + 1, z$; #3 $-x + 1/4, y + 1/4, z + 1/4$; #4 $x - 1/4, -y + 3/4, z + 1/4$; #5 $x, y, z + 1$; #6 $-x + 1/4, y - 1/4, z + 3/4$; #7 $x, y, z - 1$; $-x + 1/4, y + 1/4, z - 3/4$.

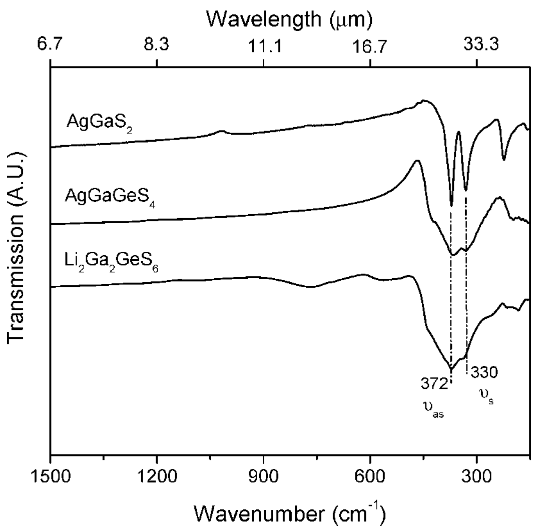

Figure 3. Infrared spectrum of polycrystalline $Li_2Ga_2GeS_6$ compared with those of $AgGaGeS_4$ and $AgGaS_2$.

and it was shown that the major peaks at 372 and 330 cm^{-1} observed in the IR spectrum were assigned to asymmetric (ν_{as}) and symmetric (ν_s) stretch vibrations of Ga−S−Ga modes, respectively, in GaS_4 tetrahedaral units. Similar features are observed in the IR spectra of $AgGaGeS_4$ and $Li_2Ga_2GeS_6$, but the absorption bands are broader than those of $AgGaS_2$, which could be related to the coexistence of GaS_4 and GeS_4 units in the $AgGaGeS_4$ and $Li_2Ga_2GeS_6$ compounds. The vibrational mode frequencies of $GeS_{4/2}$ are expected in the vicinity of those of $GaS_{4/2}$ due to the close values of the masses of Ga and Ge metal atoms. The main absorption bands were actually observed to be overlapped in many known compounds containing both GaS_4 and GeS_4 structural units.[24,25] Hence, the dominant bands located at 372 and 330 cm^{-1} in the IR spectra of $AgGaGeS_4$ and $Li_2Ga_2GeS_6$ can be assigned to the overlapped asymmetric (ν_{as}) and symmetric (ν_s) stretching of Ge−S−Ge and Ga−S−Ga modes, respectively. There are no additional absorption bands observed in the mid-IR region in both cases, which suggests that the transparent range in the mid-IR of $Li_2Ga_2GeS_6$ can be similar to that of $AgGaGeS_4$. It is reported that the single crystals of $AgGaGeS_4$ and $AgGaS_2$ are transparent up to 12 and 13 μm, respectively, in the mid-IR region. The UV/vis spectra in Figure 4 show that $Li_2Ga_2GeS_6$, $AgGaGeS_4$, and $AgGaS_2$ are transparent down to ∼0.34, ∼0.42, and ∼0.46 μm, respectively, which are the absorption edges of these compounds. The observed absorption edges of $AgGaGeS_4$ and $AgGaS_2$ measured in this experiment are comparable with 0.45 μm[10,11] for $AgGaGeS_4$ and 0.50 μm[4,6] for $AgGaS_2$. From these absorption edges, the energy band gap can be estimated to be ∼3.65 eV for $Li_2Ga_2GeS_6$, ∼2.95 eV for $AgGaGeS_4$, and ∼2.69 eV for $AgGaS_2$, respectively, which are consistent with the reported energy band gaps of 2.78 eV[8,10] for $AgGaGeS_4$ and 2.62 eV[6] for $AgGaS_2$. All of these values are listed and compared in Table 4. Because the energy band gap of optical materials is consistent with the laser damage thresholds,[26] the higher damage threshold will be obtained in the $Li_2Ga_2GeS_6$ phase compared to that of the Ag phases, which is actually observed in the following single-laser shots test.

To investigate the NLO properties of the $Li_2Ga_2GeS_6$, we performed powder SHG measurements because of the experimental difficulty in growing a suitable size and quality of a single crystal for optical measurement. When the $Li_2Ga_2GeS_6$ was probed by 1.064 μm radiations of the Nd:YAG laser, a strong SHG signal at 0.532 μm was observed, indicating that the incoming 1.064 μm photons are efficiently up-converted to 0.532 μm radiation through the $Li_2Ga_2GeS_6$. The SHG signal dependence of the particle-size of NLO

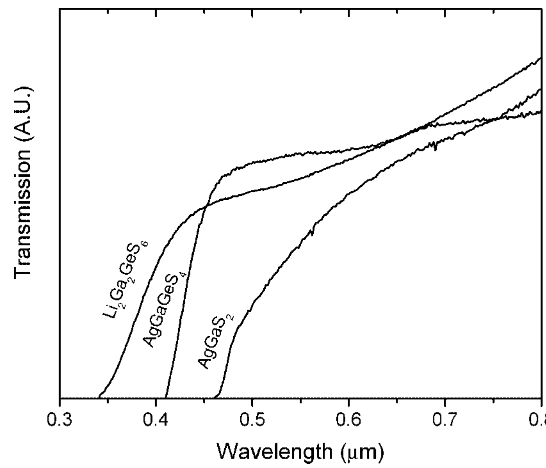

Figure 4. UV/visible spectrum of polycrystalline $Li_2Ga_2GeS_6$ and compared with those of $AgGaGeS_4$ and $AgGaS_2$.

Table 4. Optical Properties of the $Li_2Ga_2GeS_6$ Crystals Compared with those of $AgGaS_2$ and $AgGaGeS_4$ at 1.064 μm Laser Pumping

	$AgGaS_2$	$AgGaGeS_4$	$Li_2Ga_2GeS_6$
nonlinear coefficient d_{ij} (pm/V)	$d_{36} = 19$[7]	$d_{31} = 15$[10,11]	$\langle d_{eff}\rangle_{exp} = 16$[a]
absorption edges (μm) in UV/vis	∼0.46,[a] 0.50[4,6]	∼0.42,[a] 0.45[10,11]	∼0.34[a]
energy gap (eV)	∼2.69,[a] 2.62[6]	∼2.95,[a] 2.78[8,10]	∼3.65[a]
damage threshold (MW/cm^2)	20[7,8]	50[8,10,11]	

[a] Obtained from the powder samples in this experiment.

(24) Julien, C.; Barnier, S.; Massot, M.; Chbani, N.; Cai, X.; Loireau-Lozac'h, A. M.; Guittard, M. *Mater. Sci. Eng., B* **1994**, *22*, 191.
(25) Heo, J.; Yoon, J. M.; Ryou, S.Y. *J. Non-Cryst. Solids* **1998**, *238*, 115.
(26) Wu, K.; Chen, C. T. *Appl. Phys.* **1992**, *A54*, 209.
(27) Kurtz, S. K.; Perry, T. T. *J. Appl. Phys.* **1968**, *39*, 3798.

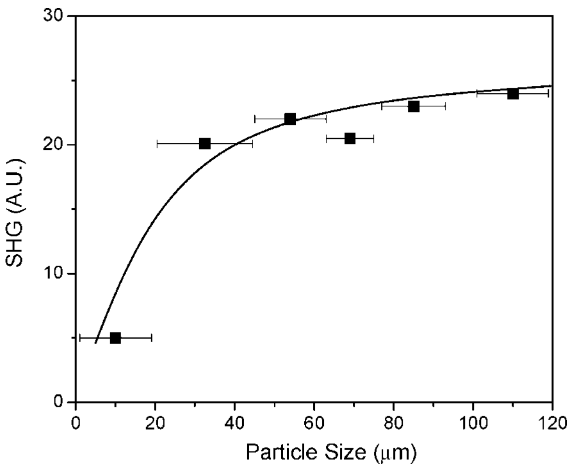

Figure 5. Phase-matching curves, i.e., particle size vs SHG intensity, for $Li_2Ga_2GeS_6$. Note that the lines are drawn to guide the eye and are not a fit to the data.

materials has been shown to be a signature of the phase-matching condition in NLO crystals[27,28] the SHG efficiency increases with the particle size and is saturated at a maximum value in the phase-matching condition. From our measurement, Figure 5, we see that the SHG signal from the $Li_2Ga_2GeS_6$ increases and is saturated at the efficiency of $200 \times I^{2\omega}_{\alpha\text{-SiO}_2}$. Using this powder SHG technique the calculation of the approximate NLO susceptibility $\langle d^{2\omega}_{ijk} \rangle$ values for powder NLO materials have been recently developed.[28] For the phase-matchable NLO crystals, the experimental average NLO susceptibilities, $\langle d_{\text{eff}} \rangle_{\text{exp}}$, have been estimated on the basis of the following equation.[28]

$$\langle d_{\text{eff}} \rangle_{\text{exp}} = \left[7.98 \times 10^2 \left(\frac{I^{2\omega}_{\text{LiGaGe}_2\text{S}_6}}{I^{2\omega}_{\text{LiNbO}_3}} \right) \right]^{1/2} \quad (2)$$

where $I^{2\omega}_{\text{LiNbO}_3}$ and $I^{2\omega}_{\text{LiGaGe}_2\text{S}_6}$ are the powder SHG efficiencies of $LiNbO_3$ and $Li_2Ga_2GeS_6$, respectively, compared to that of α-SiO_2. Because the experimentally measured $I^{2\omega}_{\text{LiNbO}_3}$ and $I^{2\omega}_{\text{LiGaGe}_2\text{S}_6}$ are 600 and 200, respectively, $\langle d_{\text{eff}}^{\text{LiGaGe}_2\text{S}_6} \rangle_{\text{exp}}$ is calculated to be 16 pm/V.

We have not observed any degradation in the SHG signal for the $Li_2Ga_2GeS_6$ under prolonged laser irradiations as evidenced by the continued strong production of 0.532 μm light. On the other hand, the SHG efficiency of the $AgGaGeS_4$ was observed to be $\sim 20 \times I^{2\omega}_{\alpha\text{-SiO}_2}$ at initial laser shots, but it lost about 90% of its SHG efficiency after $\sim$ 100 laser pulses. The $AgGaS_2$ immediately decomposed (darkened) after showing very low intensity of SHG ($1 \times I^{2\omega}_{\alpha\text{-SiO}_2}$) and then eventually even this SHG intensity disappeared completely. This quantitative test reveals that the $Li_2Ga_2GeS_6$ was not damaged under our pumping laser system, Nd:YAG 1.064 μm laser with 3 mW power, whereas $AgGaGeS_4$ and $AgGaS_2$ are significantly unstable under the same conditions. The specific laser damage thresholds of the $AgGaGeS_4$ and $AgGaS_2$ have been reported to be 50 and 25 MW/cm^2 for $\lambda = 1.064$ μm under identical conditions,[8] which agree well with the results of the above quantitative tests.

Hence, the $Li_2Ga_2GeS_6$ will have a higher laser damage threshold than the $AgGaGeS_4$, which is also supported by the shorter absorption edge observed in UV/visible range in Figure 4. Because the $Li_2Ga_2GeS_6$ and $AgGaGeS_4$ have the same framework structure based on the corner sharing of GaS_4 with GeS_4 tetrahedra, the different laser damage threshold could be induced by the chemistry of the different cations, Li and Ag, that are located in the interstitial space. It is generally known that many Ag compounds show photodarkening because of the photo-assisted reduction processes of the Ag^+. This is a likely reason why Ag-based NLO materials have noticeably lower laser damage thresholds than what is often required.

Conclusions

We have synthesized the noncentrosymmetric compound $Li_2Ga_2GeS_6$ and determined its structure and its optical transmission range as well as its NLO SHG properties. The $Li_2Ga_2GeS_6$ is phase-matchable with a SHG efficiency of approximately $200 \times \alpha$-SiO_2. In addition, its high laser damage threshold makes it very stable under prolonged Nd: YAG 1.064 um laser irradiation. Based on the strong SHG intensity with high laser damage threshold $Li_2Ga_2GeS_6$ can serve as an intracavity frequency doubler in so-called “self-frequency doubling solid state lasers”. Because the use of $Li_2Ga_2GeS_6$ in practical applications depends on growing large optical quality single crystals, further studies are planned to grow a single crystals of $Li_2Ga_2GeS_6$ and fully characterize its optical properties.

Acknowledgment. The authors thank Dr. Arkady Ellern with the Chemistry Instrumentation Facility at the Molecular Structure Laboratory of Iowa State University for collecting the single-crystal X-ray diffraction data. P.S.H. and J.B. thank the NSF (DMR-0652150) and the Welch Foundation for support. N.A. and H.S. thank the Welch Foundation of Houston, TX, for support under Grant F-273.

Supporting Information Available: Crystallographic file in CIF format for $Li_2Ga_2GeS_6$; measured and calculated powder XRD pattern of $Li_2Ga_2GeS_6$ (PDF). This material is available free of charge via the Internet at http://pubs.acs.org.

CM8007304

(28) Ok, K. M.; Chi, E. O.; Halasyamani, P. S. *Chem. Soc. Rev.* **2006**, *35*, 710.